Behavioral/Cognitive

The Occipital Place Area Is Recruited for Echo-Acoustically Guided Navigation in Blind Human Echolocators

Liam J. Norman and Lore Thaler
Department of Psychology, Durham University, Durham DH1 3LE, United Kingdom

In the investigation of the brain areas involved in human spatial navigation, the traditional focus has been on visually guided navigation in sighted people. Consequently, it is unclear whether the involved areas also support navigational abilities in other modalities. We explored this possibility by testing whether the occipital place area (OPA), a region associated with visual boundary-based navigation in sighted people, has a similar role in echo-acoustically guided navigation in blind human echolocators. We used fMRI to measure brain activity in 6 blind echolocation experts (EEs; five males, one female), 12 blind controls (BCs; six males, six females), and 14 sighted controls (SCs; eight males, six females) as they listened to prerecorded echolocation sounds that conveyed either a route taken through one of three maze environments, a scrambled (i.e., spatio-temporally incoherent) control sound, or a no-echo control sound. We found significantly greater activity in the OPA of EEs, but not the control groups, when they listened to the coherent route sounds relative to the scrambled sounds. This provides evidence that the OPA of the human navigation brain network is not strictly tied to the visual modality but can be recruited for nonvisual navigation. We also found that EEs, but not BCs or SCs, recruited early visual cortex for processing of echo acoustic information. This is consistent with the recent notion that the human brain is organized flexibly by task rather than by specific modalities.

Key words: **audition; blindness; echolocation; fMRI; route recognition**

Significance Statement

There has been much research on the brain areas involved in visually guided navigation, but we do not know whether the same or different brain regions are involved when blind people use a sense other than vision to navigate. In this study, we show that one part of the brain (occipital place area) known to play a specific role in visually guided navigation is also active in blind human echolocators when they use reflected sound to navigate their environment. This finding opens up new ways of understanding how people navigate, and informs our ability to provide rehabilitative support to people with vision loss.

Introduction

Human spatial navigation involves a network of brain areas, reflecting the different components involved in navigation (Ekstrom et al., 2017; Kong et al., 2017; Boccia et al., 2014). What is unclear, however, is whether these areas serve a role that is specific to whichever modality is most dominantly used for navigation (typically vision in humans), or whether they serve a more general role that could accommodate another modality entirely. Indeed, there is an increasing amount of evidence to suggest that the human brain is organized flexibly by task rather than by sensory modality (Amedi et al., 2017); that is, a given brain area can serve the same function across different input modalities.

Visual perception has been at the forefront of navigation research in humans because of the uniquely salient role of visual information (Ekstrom et al., 2017; Chan et al., 2012; Ekstrom, 2015). That is not to say, however, that nonvisual information could also be used. For example, people who are blind are also capable of excellent spatial navigation (Thinus-Blanc and Gaunet, 1997; Loomis et al., 2001). Rather, it is poorly understood whether such nonvisual navigational abilities involve the same brain processes as visual-based navigation (Fiehler et al., 2015; Kupers et al., 2010; Maidenbaum et al., 2018).

To address this, we must identify whether brain areas with specific roles in visual-based navigation have equivalent roles during nonvisual navigation. One brain region in particular, the occipital place area (OPA), is known to provide the perceptual source of environmental boundary information that guides navigation through that environment (Kamps et al., 2016; Julian et al., 2016). Furthermore, because the OPA is located near the transverse occipital sulcus, it is assumed that this perceptual

Received July 20, 2022; revised Mar. 9, 2023; accepted Mar. 14, 2023.

Author contributions: L.J.N. and L.T. designed research; L.J.N. and L.T. performed research; L.J.N. analyzed data; and L.J.N. and L.T. wrote the paper.

This work was supported by United Kingdom Research and Innovation–Biotechnology and Biological Sciences Research Council Grant BB/M007847/1 to L.T.

The authors declare no competing financial conflicts.

Correspondence should be addressed to Liam J. Norman at liam.norman@durham.ac.uk or Lore Thaler at lore.thaler@durham.ac.uk.

https://doi.org/10.1523/JNEUROSCI.1402-22.2023

representation emerges from visual input. Human echolocation offers a well-suited model in which to test whether the OPA has a similar navigational role in a nonvisual modality. Echolocation is the ability to perceive objects and space through sound echoes (Griffin, 1944) and offers the ability to perceive the proximal and distal environment. Some people who are blind use click-based echolocation (i.e., echolocation using mouth clicks) to perceive the position of an object in space as well as its shape, material, and whether it is in motion (for review, see Kolarik et al., 2014; Thaler and Goodale, 2016). Furthermore, using echolocation for these purposes is associated with neural activity in areas that are typically associated with perceiving those same properties through vision (Norman and Thaler, 2019; Thaler et al., 2011; Arnott et al., 2013; Milne et al., 2015; Thaler et al., 2014).

We used fMRI to measure brain activity in 6 blind echolocation experts (EEs), 12 blind controls (BCs), and 14 sighted controls (SCs) as they listened to prerecorded binaural echolocation sounds (i.e., echo-acoustic sound through a first-person perspective) and made perceptual judgments about them. The critical contrast in our analysis was to compare brain activity during coherent route sounds to activity during scrambled (i.e., spatiotemporally incoherent) sounds. This design is an echo-acoustic analog of one used previously to identify OPA activity during visually guided navigation (Kamps et al., 2016).

We used a region of interest (ROI) analysis approach, focusing on the OPA in addition to the parahippocampal place area (PHPA) because of its role in the neural representation of places and scenes (Epstein et al., 1999) and the superior parietal lobule (SPL) because of its previously identified activation in some nonvisual navigation tasks (Kupers et al., 2010; Fiehler et al., 2015). We also included ROIs for primary visual (V1) and auditory (A1) areas to analyze activity in low-level sensory processing areas and also because there is some evidence that V1 is active during nonvisual navigation (Maidenbaum et al., 2018). In addition to the ROI analysis, we also ran a whole-brain analysis.

Part of the data (behavioral performance outside the scanner for SCs and three EEs) has been reported previously (Dodsworth et al., 2020).

Materials and Methods

Ethics. All procedures followed the British Psychological Society Code of Practice and the World Medical Association Declaration of Helsinki. The experiment had received ethical approval by the Ethics Advisory Subcommittee in the Department of Psychology at Durham University (Reference 14/13). All participants gave written informed consent to take part in this study. Participants who were sighted and participants who were blind received £6/h and £10/h, respectively, to compensate them for their effort and time.

Participants. All participants were recruited through word of mouth and opportunity sampling. Six blind expert echolocators (EEs; five males, one female) took part (Table 1). Our requirement for classing an individual as an echolocation expert was that they reported using click-based echolocation on a daily basis for more than 10 years. In our sample, five of the six EEs had cause of vision loss present from birth and were diagnosed as legally blind from birth or within the first year of life. The remaining EE (EE4) received an official diagnosis age 12 because of sudden vision loss. Thus, the majority of our echolocation expert participants are classified as early blind.

Twelve BCs (six males, six females) with no prior experience in click-based echolocation took part in the study (Table 1). In our sample, all BCs had cause of vision loss present from birth. All were diagnosed as legally blind in childhood, with only two official diagnoses at an age that might have coincided with onset of puberty or may have been after onset of puberty (i.e., 13 years and 10 years; BC9 and BC2) but again with vision impairment having been present from birth. Thus, the majority of our participants were classified as early blind. All our blind participants were independent travelers, and all had received mobility and orientation training as part of visual impairment (VI) habilitation, which is provided to people with VI in the UK. Fourteen SCs (eight males, six females) took part (ages, 21, 21, 22, 22, 23, 24, 25, 27, 32, 35, 38, 48, 60, and 71 years; mean, 33.5 years; SD, 15.8 years; median, 26 years). All reported to have normal or corrected-to-normal vision and no prior echolocation experience (based on self-report).

All participants had normal hearing appropriate for their age group (International Organization for Standardization 7029:2017) as assessed using pure tone audiometry, with the exception of one blind participant (BC6, age 72 years), who wore hearing aids to compensate for age-related hearing loss. For purposes of testing, the participant with hearing aids did not wear the aids during any of the experimental testing sessions because the participant would not be able to wear these in the MRI scanner. For our statistical analyses that involve comparisons with the BC group, we report the results of those analyses both with and without BC6 included. All participants who had any residual vision were tested under blindfold.

Experimental design and statistics. The design contained a between-subject variable (subject group) and within-subject variable (sound stimulus). Full details of the statistical analyses of the behavioral, ROI, and whole-brain data are given in the relevant sections below. To summarize briefly, behavioral and ROI data were analyzed using ANOVAs and Kruskal–Wallis tests and, where appropriate, one-sample t tests and Wilcoxon signed-rank tests. The issue of multiple comparisons was addressed using either Bonferonni correction or the Benjamini–Hochberg method. Whole-brain fMRI data were analyzed using ANOVAs and one-sample t tests, with cluster-based thresholding and Gaussian random field correction (Worsley, 2001).

Echolocation stimuli. The stimuli were created from a large set of recordings first described by Dodsworth et al. (2020), which contains full details of those stimuli. Briefly, binaural recordings of clicks and click echoes were made with an anthropometric mannequin in physical spaces comprising corridors in specific spatial arrangements (T-mazes, U-mazes, Z-mazes). Details of the mannequin have been reported in a previous study (Norman and Thaler, 2018). In addition, we also created spatially mirrored versions of these recordings by flipping the left and right channels, giving six maze layouts in total.

For each of the six mazes, we created two samples by selecting recordings corresponding to a specific sequence of locations and orientations within that maze (Fig. 1). This gave a total of 12 sound files that were each 10.53 s in length and contained 18 clicks and echoes, each separated by 600 ms (a rate of 1.71 clicks/s). These 12 sound files were assigned to one of three categories, single-turn route, two-turn route in same direction, and two-turn route in different (opposite) directions.

In addition to these spatially coherent route sounds, we created two types of control sounds: scrambled route sounds and clicks with no echoes. A scrambled route sound was created for each of the original route sounds to create sounds that had exactly the same low-level acoustic information (i.e., timing, clicks, and echoes) but did not convey spatially coherent information. To do this, the individual click-echo sounds in each route sound file were randomly shuffled and pieced together (maintaining the same click rate) so that there was no coherent route. To create a secondary set of control stimuli (i.e., stimuli with clicks but not containing any echoes), a sound recording was used during which the mannequin had been placed facing the foam padded wall in the anechoic chamber. The sound was then repeated at the same temporal sequence as that for the route and scrambled sound files.

In total, five types of sound stimuli were created: single-turn route, two-turns-same route, two-turns-different route, scrambled route, and click only. Example WAV files for each of these stimuli can be found on Open Science Framework (https://osf.io/c5pn2/), but note that playback of these example sounds should be done using a high-specification sound card and headphones because of the nature of the echolocation sounds.

Stimuli containing echoes (route and scrambled stimuli) were of higher root mean square intensity than stimuli not containing echoes (no echo). Specifically, for T and T-scrambled maze sounds, −41.4 dB;

Table 1. Details of all blind participants, organized by group

Participant	Sex	Age	Degree of vision loss	Cause and age of vision loss	Echolocation use
EE1	M	53	Total blindness	Enucleation because of retinoblastoma at 13 months	Daily, since early childhood/no exact age remembered
EE2	M	60	Bright light detection both eyes	Retinal detachment from birth	Daily, since 6 years old
EE3	M	49	Total blindness	Enucleation because of retinoblastoma at 18 and 30 months	Daily, since 8 years old
EE4	M	24	Total blindness	Vision loss suddenly at age 12 years because of unknown causes, enucleation at age 19 years to alleviate ocular discomfort	Daily, since 12 years old
EE5	M	37	Total blindness	Gradual sight loss since birth because of glaucoma	Daily, since 12 years old
EE6	F	43	Total blindness	Leber's congenital amaurosis, from birth	Daily, since 31 years old
BC1	F	60	Total blindness in left eye, some peripheral vision in right eye	Stichler's syndrome, retinal sciasis from birth with increasing severity	Some experience, very little regular use
BC2	M	38	Tunnel vision (<2°) and decreased acuity (<20/200) in both eyes	Retinitis pigmentosa and other retinal pathology (unknown), official diagnosis in early childhood (no exact age remembered but was known when commencing school, i.e., age 5 years)	None
BC3	M	54	Residual bright light perception	Retinitis pigmentosa, official diagnosis age 10 years, gradual sight loss from birth	Some experience, very little regular use
BC4	M	39	Residual bright light perception	Retinitis pigmentosa, gradual sight loss from birth, official diagnosis in early childhood (no exact age remembered but was known when commencing school, i.e., age 5 years)	None
BC5	F	44	Total blindness right eye, bright light detection left eye	Micropthalmia and glaucoma, right eye enucleated age 39 years	None
BC6	F	72	Bright light detection	Retinitis pigmentosa, gradual sight loss from birth, official diagnosis in early childhood (no exact age remembered but was known when commencing school, i.e., age 5 years)	None
BC7	M	46	Total blindness	Ocular albinism, gradual sight loss from birth	Some experience, very little regular use
BC8	F	36	Bright light detection	Unknown cause, from birth.	None
BC9	M	37	Tunnel vision (<5°) and decreased acuity (<20/200) in both eyes.	Retinitis pigmentosa, gradual sight loss from birth, official diagnosis at age 13 years	None
BC10	F	27	Left eye ~1° of foveal vision left with reduced acuity (<20/200), right eye bright light detection	Leber's amaurosis and cataracts from birth	None
BC11	F	79	Some blurred foveal vision, prone to bleaching	Rod cone dystrophy from birth.	None
BC12	M	48	Total blindness in left eye, residual bright light perception in right eye	Severe childhood glaucoma from 3 months old	None

F, Female; M, male.

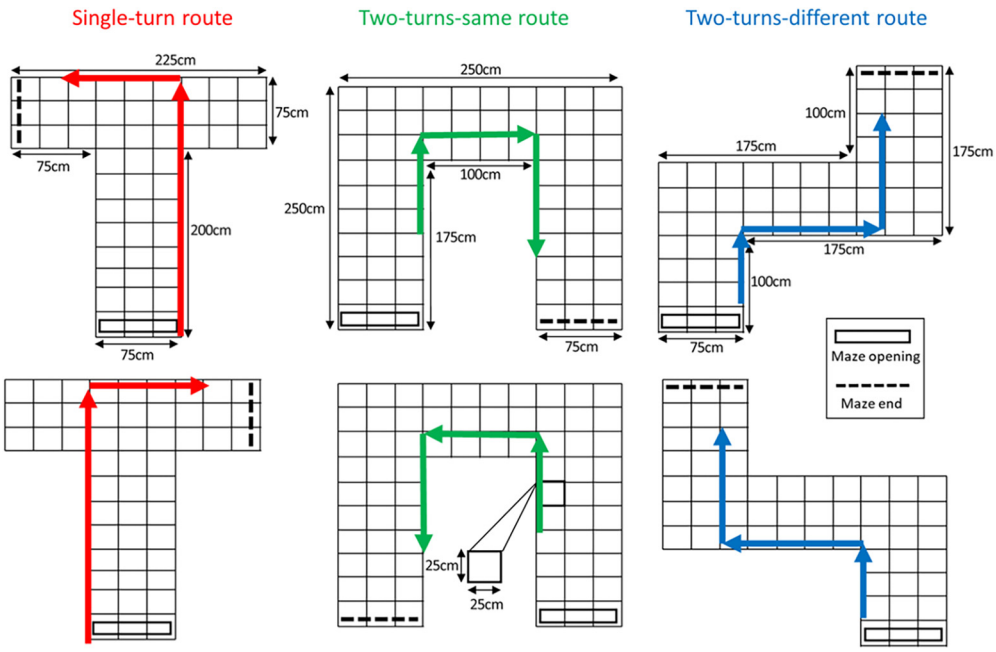

Figure 1. Illustration of spatial arrangements used to construct virtual spaces (T-mazes, U-mazes, Z-mazes) and the prespecified routes taken through each one. Each route was composed of 18 click recordings taken at regularly spaced intervals. Specifically, there was one click for each position along the route (marked by the intersections) and two clicks for each rotation of 90° (in 45° steps).

for U and U-scrambled maze sounds, −41.4 dB; for Z and Z-scrambled maze sounds, −40.8 dB; for no-echo sounds, −44.2 dB. In terms of absolute intensity at which sounds were played, each participant selected a sound intensity that felt comfortable to do the task. The same intensity was maintained for that participant throughout testing. Recorded sound files were filtered to achieve frequency response equalisation for playback through the MRI-compatible insert earphones (Model S-14, Sensimetrics, Malden, MA; filters provided by the manufacturer).

Behavioral paradigm before fMRI scanning. On a separate day before fMRI scanning, participants completed two runs of 30 trials. On each trial they heard one of the sound stimuli from one of the five categories (single-turn route, two-turns-same route, two-turns-different route, scrambled, and no echo), with each condition being repeated six times. The order of trials was randomly determined at the start of each run. When the sound finished playing, participants gave a verbal response to indicate which category the sound belonged to. The experimenter recorded this response and started the next trial. Before participants performed the two runs of 30 trials, they were played two examples for each type of sound to make them familiar with the sounds and the required responses.

Setup and apparatus before fMRI scanning. Participants completed the task in a sound-insulated and echo-acoustic dampened room (~2.9 × 4.2 × 4.9 meters) lined with foam wedges (cutoff frequency 315 Hz) in the Department of Psychology at Durham University. Sounds were played through MRI-compatible insert earphones (Model S-14, Sensimetrics, Malden, MA; filters provided by the manufacturer) encased in disposable foam tips the earphones provided 20 to 40-dB attenuation of external sound, connected to a Kramer 900N Stereo Power Amplifier, with input provided by a USB soundcard (Creative Sound Blaster X-Fi HD Sound Card, Creative Technology). The experimenter used a laptop (Dell Latitude E7470, Intel Core i56300U CPU 2.40. 8GB RAM, 64-bit Windows 7 Enterprise) running MATLAB R2018b (MathWorks) and modified functions from the Psychtoolbox library (Brainard, 1997) to control sound playback and to record participants' responses.

Behavioral paradigm during fMRI scanning. Participants' task inside the scanner was the same as that outside the scanner, with some modifications. Participants gave their response after each stimulus presentation by pressing one of five buttons on an MR-compatible response unit (Five-Button Fiber Optic Response Button System, Psychology Software Tools). Each finger was assigned a different response (thumb, no echo; index, single turn; middle, two turns same; ring, two turns different; pinkie, scrambled). A beep (1.2 kHz, 50 ms) at the end of the stimulus presentation prompted participants to respond. In addition to the five stimulus categories, a sixth silence category was also used (to allow comparisons to baseline activity in the fMRI data analysis). During these silence trials, no sound was played to participants, and no response was required. The order of stimulus presentation was counterbalanced with respect to the three main stimulus conditions (route, scrambled, and no echo). This was achieved by breaking down 36 trials in each run into 9 sequential groups of 4. The first trial in each group was always a silence trial, and the remaining three were a random order of route, scrambled, and no echo. The order of these three trial types was counterbalanced so that after every two runs, each type was presented equally often in each of the three sequence positions. The same randomized order of sounds was used for all participants.

Setup and apparatus during fMRI scanning. All MR data were acquired at Durham University Center for Imaging (James Cook University Hospital, Middlesbrough, UK), with a 3-tesla, whole-body MRI system (Magnetom Tim Trio, Siemens) and a 32-channel head coil. For sound presentation the same equipment as that used before fMRI scanning was used to play sounds, with the exception that a PC (Intel Core i7-6700 CPU 3.40, 8GB RAM, 64-bit Windows 7 Enterprise) was used instead of a laptop. Further, participants gave their response using an MRI-compatible five-Button Fiber-Optic Button Response Unit (Psychology Software Tools) with their right hand. To minimize background noise, the circulatory air fan of the MRI bore was turned off during experimental runs. To minimize interference from light sources, all lights inside the MRI room were turned off, and participants who were not totally blind wore a blindfold.

fMRI scanning parameters. High-resolution structural images for each participant were acquired using a T1-weighted, optimized sequence (MPRAGE), at a resolution of 1 × 1 × 1 mm. Functional images were acquired using a single-shot gradient echoplanar pulse sequence in combination with a sparse sampling design (Hall et al., 1999), with a repetition time of 13 s (11 s of inactivity for stimulus presentation, followed by 2 s of volume acquisition). Thus, during stimulus presentation, no functional volumes were acquired. Instead, a single functional volume was acquired in the 2 s period after the end of stimulus presentation. Field of view was 192 mm with a matrix size of 64 × 64, giving an in-slice resolution of 3 mm. Thirty-eight contiguous axial slices were acquired in ascending order with a slice thickness of 3.5 mm, covering the whole brain. Echo time was 30 ms and flip angle was 90°. For each run, a total of 38 functional volumes were acquired, with each run lasting 8 min and 14 s. The first and last volume in each run were acquired after silence. A total of six runs were completed per participant, except for one participant (BC2), who completed only four runs.

fMRI data processing. FMRI data preprocessing and analysis was conducted using Functional MRI of the Brain (FMRIB) fMRI Expert Analysis Tool (FEAT) version 6.00, part of the FMRIB Software Library (FSL; www.fmrib.ox.ac.uk/fsl; Woolrich et al., 2001, 2004)

Images were brain extracted (using the Brain Extraction Tool; Smith, 2002), and within-participant registration of low-resolution functional images to high-resolution structural (T1) images was achieved using FMRIB Linear Image Registration Tool (FLIRT; 6 df; Jenkinson et al., 2002; Jenkinson and Smith, 2001). Further nonlinear registration to MNI 152 standard space (voxel size of 2 mm) was achieved using FNIRT (FMRIB Nonlinear Registration Tool; Andersson et al., 2010) with a warp resolution of 2 mm. The very first functional volume within each run was discarded, leaving 37 volumes to analyze, the first and last of which were acquired after silence. The following prestatistic processing was applied to each run of functional data: slice-timing correction using Hanning-Windowed Sinc Interpolation, motion correction using MCFLIRT (FMRIB Linear Image Registration Tool with motion correction; Jenkinson et al., 2002), high-pass temporal filtering (maximum allowed period, 100 s or 0.01 Hz), and spatial smoothing (full-width at half maximum Gaussian kernel of 5 mm).

fMRI modeling and contrasts. In the first-level analysis for each run, three explanatory variables (EVs) were modeled using stick function regressors (with no hemodynamic response convolution because of the sparse sampling design)—stimulus, scrambled stimulus, and no-echo stimulus. The silence trials were used as an implicit baseline. These EVs were then used to define the three contrasts of interest: route versus scrambled (EV weights, route = +1, scrambled = −1, no echo = 0), echo versus no echo (EV weights, route = +1, scrambled = +1, no echo = −2), and sound versus silence (EV weights, route = +1, scrambled = +1, no echo = +1).

In a second-level analysis stage, single-participant activations across all runs were calculated using a fixed effects model by forcing the random effects variance to zero in FLAME (FMRIB Local Analysis of Mixed Effects; Beckmann et al., 2003; Woolrich et al., 2004; Woolrich, 2008). In a higher-level analysis stage, group-level activations were calculated using a mixed effects model.

ROI definition and analysis. Five ROIs were defined in standard MNI space (Table 2). Contrasts analyzed for each ROI were (1) route versus scrambled, (2) echo versus no-echo, and (3) sound versus silence. FSL Featquery was used to extract the percentage signal change (PSC) associated with each of the three contrasts for each ROI for each participant.

Whole-brain analysis. In addition to the ROI analysis, we also ran a series of whole-brain analyses. First, we ran a between-subject ANOVA to identify brain areas in which there was a significant difference among the three groups (i.e., testing whether EE = BC = SC) for each stimulus contrast. Following this, we calculated averages for each group (i.e., one-sample *t* tests) for each contrast (same as those used in the ROI analysis). *Z* statistic images (Gaussianized *t*/*F*) were thresholded using cluster-based thresholding determined by $Z > 2.3$ and a cluster significance threshold of $p = 0.05$ (corrected using Gaussian random field theory; Worsley, 2001).

To objectively assign anatomic labels to activation clusters, the coordinates of the peak activity within each cluster were extracted along with

Table 2. ROI details

ROI label	Description
A1	Primary auditory cortex, based on areas TE 1.0, 1.1, and 1.2 in the Jülich histologic (cytoarchitectonic and myeloarchitectonic) atlas (threshold >50%)
V1	Primary visual cortex, based on area 17/V1 in the Jülich histologic (cytoarchitectonic and myeloarchitectonic) atlas (threshold >50%)
OPA	Sphere of 7.5 mm radius at approximate location of the OPA, based on average MNI coordinates (left, −29.4, −83.8, 23.9; right, 35.7, −78.5, 23.7; provided by Sun et al., 2021). These coordinates were acquired using a localizer comparing scenes versus objects, averaged across 17 participants
PHPA	Parahippocampal place area (PHPA) based on probabilistic atlas from Weiner et al. (2018), fitted to the MNI standard template
SPL	Superior parietal lobule (SPL) based on the combination of subareas 5 Ci, 5L, 5 M, 7A, 7 M, 7P, and 7PC in the Jülich histologic (cytoarchitectonic and myeloarchitectonic) atlas (threshold >50%).

For each named ROI, data were averaged across the left and right hemispheres (unless stated otherwise). Where a probabilistic atlas was used to define the ROI, the classification threshold is given (i.e., only voxels with a probabilistic value above this threshold were included).

the coordinates of the local maxima within each cluster, and these was used to extract corresponding labels from the Jülich histologic cytoarchitectonic atlas (Eickhoff et al., 2007) and MNI structural atlas (Collins et al., 1995; Mazziotta et al., 2001). Where the atlases returned probabilistic values of at least 25% for a particular anatomic label, this label was then assigned to that cluster.

Results

Behavioral

For the data collected before MR scanning, we calculated the proportion of correct responses for three different measures of performance—specific route identification, route versus scrambled identification, and echo identification. One-way ANOVAs (with subject group as the between-subject variable) were used to test for group differences for each of these measures in performance, reported below (in addition to nonparametric Kruskal–Wallis tests). Behavioral performance during fMRI was also analyzed in the same way, and the pattern of results was consistent with what we observed before scanning. We found the in-scanner measure to be more variable, however, because of participants pressing more than one key accidentally or failing to respond on some trials.

Specific route identification

When considering specific route identification, a response was correct when participants identified the specific route (single turn, two turns same, two turns different) when it was presented. Thus, specific route identification measures participants' ability to correctly identify specific echo-acoustic routes. There was a significant group difference in route identification ($F_{(2,29)}$ = 26.159, $p < 0.001$, $\eta^2 = 0.643$; Kruskal–Wallis, $H_{(2)}$ = 13.830, $p < 0.001$). EEs (mean = 0.806) were significantly more accurate than BCs (mean = 0.475; $p < 0.001$; and $p < 0.001$ with BC6 excluded) and SCs (mean = 0.470; $p < 0.001$). BCs and SCs were not significantly different from one another ($p = 1.000$). These data are shown in Figure 2*A*.

Route versus scrambled identification

When considering scrambled versus route identification, a response was identified as correct when participants gave a scrambled response to a scrambled sound but also when they gave any of the route responses when any of the route sounds were presented (regardless of whether it was a single turn, two turn same, or two turn different). Thus, scrambled versus route identification measures participants' ability to distinguish spatially coherent echo-acoustic sounds from spatially incoherent echo-acoustic sounds. There was a significant group difference in this measure ($F_{(2,29)}$ = 10.681, $p < 0.001$, η^2 = 0.424; Kruskal–Wallis, $H_{(2)}$ = 13.719, $p < 0.001$). EEs (mean = 0.962) were significantly more accurate than BCs (mean = 0.790; $p = 0.001$; and $p = 0.002$ with BC6 excluded) and SCs (mean = 0.784; $p < 0.001$). BCs and SCs were not significantly different from one another ($p = 1.000$). These data are shown in Figure 2*B*.

Echo versus no-echo identification

When considering echo identification, a response was identified as correct when participants responded with no echo when stimuli containing no echoes were present and also when participants gave any other response when any of the other stimuli were presented (e.g., if a single-turn route was labeled as scrambled, then this would be classed as correct because the sound contains echoes). Thus, echo identification measures participants' ability to distinguish echo from nonecho sounds. There was no significant group difference in this measure ($F_{(2,29)}$ = 2.507, $p = 0.099$; Kruskal–Wallis, $H_{(2)}$ = 3.710, $p = 0.156$). This is likely because all groups had very high accuracy (EEs mean = 1.000; BCs mean = 0.963; SCs mean = 0.986). This high level of performance in detecting the presence of echoes even for naive echolocators is consistent with our previously published results (Norman and Thaler, 2020; 2021). These data are shown in Figure 2*C*.

Overall, these results suggest that EEs as a group performed better than both BCs and SCs for those measures where spatial interpretation of echo information was required (i.e., route vs scrambled and route identification) but not for simple echo detection. Also, BCs and SCs did not perform differently from one another on any measure, suggesting that experience with echolocation rather than blindness drives performance in this task.

fMRI: ROI analysis

The group means for all contrasts are shown in Figure 3, and the individual data for the six EEs are shown in Table 3. We tested for group differences in PSC for each ROI and for each contrast using one-way ANOVAs (subject group as the between-subject variable) and nonparametric Kruskall–Wallis tests. Each resulting p value was Bonferroni corrected by multiplying it by five (the number of ROIs). Any results in which these corrected p values were <0.05 are reported as significant (thus, the alpha level was effectively 0.0083). *Post hoc* tests were also Bonferroni corrected by a factor of three (the number of multiple comparisons). One-sample t tests and nonparametric Wilcoxon signed-rank tests were also used to test whether PSC in each ROI was significantly different from zero. The issue of multiple comparisons was addressed using the Benjamini–Hochberg method to control false discovery rate (FDR; set at 0.05; Benjamini and Hochberg, 1995). This was chosen over the highly conservative Bonferroni adjustment because of the large number of tests (15 for each contrast). Briefly, this method involves ranking the observed p values in order of size and calculating a Benjamini–Hochberg critical value for each one (based on the rank number and the FDR). Any p values that are less than the critical value for their rank are considered to be statistically significant. Thus, the p values reported for these tests are not adjusted per se, but results are only reported as significant where the p values were less than the Benjamini–Hochberg critical value.

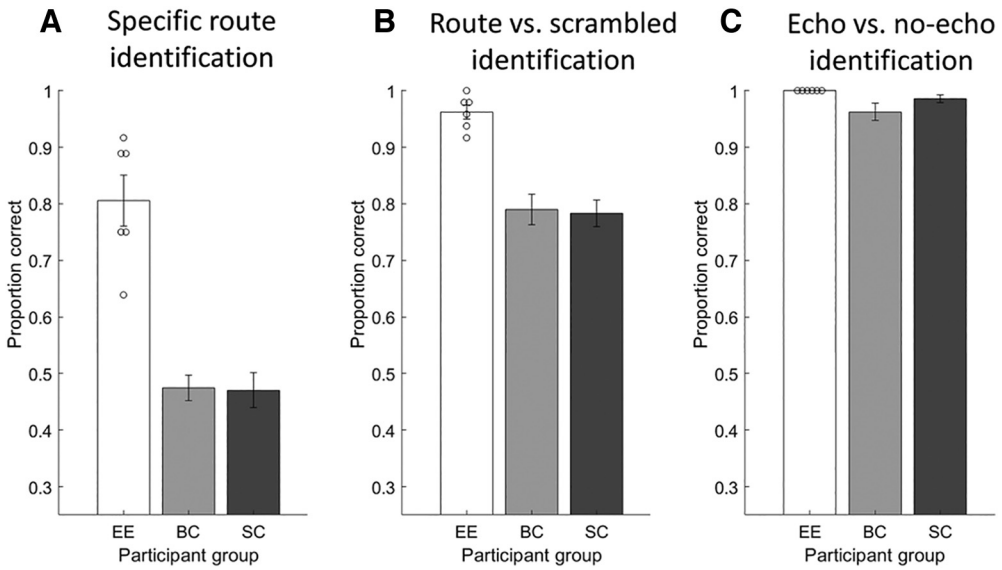

Figure 2. Data from the behavioral task conducted before the fMRI task. ***A–C***, Three separate measures of performance are given—ability of participants to identify specific route types (***A***), identify coherent route sounds versus scrambled sounds (***B***), and identify the sounds containing echoes from those that do not (***C***). Error bars indicate SEM. Circles illustrate performance of individual EEs.

Route versus scrambled

For the route versus scrambled contrast, a significant group difference was found in the OPA ($F_{(2,29)} = 13.344$, $p < 0.001$, $\eta^2 = 0.479$; Kruskal–Wallis, $H_{(2)} = 12.370$, $p = 0.010$). The EE group showed significantly greater PSC than the BC ($p = 0.001$; and $p = 0.002$ with BC6 excluded) and SC ($p < 0.001$) groups. The BC and SC groups did not differ ($p = 0.732$; and $p = 0.657$ with BC6 excluded). None of the other ROIs showed a significant difference between groups (A1, $F_{(2,29)} = 0.266$, $p = 1.000$; Kruskal–Wallis, $H_{(2)} = 0.401$, $p = 1.000$; V1, $F_{(2,29)} = 0.563$, $p = 1.000$; Kruskal–Wallis, $H_{(2)} = 1.167$, $p = 1.000$; PHPA, $F_{(2,29)} = 0.636$, $p = 1.000$; Kruskal–Wallis, $H_{(2)} = 1.289$, $p = 1.000$; SPL, $F_{(2,29)} = 1.405$, $p = 1.000$; Kruskal–Wallis, $H_{(2)} = 1.791$, $p = 1.000$).

PSC in the OPA was significantly greater than zero for the EE group ($t_{(5)} = 5.591$, $p = 0.003$; Wilcoxon signed rank, $z = 2.201$, $p = 0.028$). No other tests showed a significant difference from zero.

Our SCs were, on average, younger than our EEs. To test the possibility that age might be a determining factor in the strength of response in the OPA, we correlated age with the route versus scrambled response in the OPA in our SC groups and found no significant association ($r_{(12)} = 0.316$, $p = 0.272$).

Echo versus no echo

A significant group difference was found in V1 ($F_{(2,29)} = 14.837$, $p < 0.001$, $\eta^2 = 0.506$; Kruskal–Wallis, $H_{(2)} = 13.479$, $p = 0.006$). The EE group showed significantly greater PSC than the BC ($p < 0.001$; and $p = 0.001$ with BC6 excluded) and SC ($p < 0.001$) groups. The BC and SC groups did not differ ($p = 0.824$). A significant group difference was also found in the OPA ($F_{(2,29)} = 14.979$, $p < 0.001$, $\eta^2 = 0.508$; Kruskal–Wallis, $H_{(2)} = 14.779$, $p = 0.003$). The EE group showed significantly greater PSC than the BC ($p = 0.005$; and $p = 0.005$ with BC6 excluded) and SC ($p < 0.001$) groups. The BC and SC groups did not differ ($p = 0.072$). None of the other ROIs showed a significant group effect (A1, $F_{(2,29)} = 2.443$, $p = 0.523$; Kruskal–Wallis, $H_{(2)} = 5.643$, $p = 0.298$; PHPA, $F_{(2,29)} = 4.818$, $p = 0.078$; Kruskal–Wallis, $H_{(2)} = 11.388$, $p = 0.017$; SPL, $F_{(2,29)} = 1.618$, $p = 1.000$; Kruskal–Wallis, $H_{(2)} = 3.632$, $p = 0.814$).

PSC in V1 was significantly greater than zero for the EE group ($t_{(5)} = 4.628$, $p = 0.006$; Wilcoxon signed rank, $z = 2.201$, $p = 0.028$). PSC in A1 was significantly greater than zero for the SC group ($t_{(13)} = 5.641$, $p < 0.001$; Wilcoxon signed rank, $z = 3.233$, $p = 0.001$). PSC in PHPA was significantly lower than zero for the SC group ($t_{(13)} = 5.282$, $p < 0.001$; Wilcoxon signed rank, $z = 2.982$, $p = 0.003$). No other tests showed a significant difference from zero.

Sound versus silence

A significant group difference was found in V1 ($F_{(2,29)} = 5.872$, $p = 0.036$, $\eta^2 = 0.288$; but note Kruskal-Wallis was not significant, $H_{(2)} = 8.228$, $p = 0.082$). The EE group showed significantly greater PSC than the SC group ($p = 0.006$) but not the BC group ($p = 0.050$; and $p = 0.086$ with BC6 excluded). The BC and SC groups did not differ ($p = 0.180$). A significant group difference was also found in the OPA ($F_{(2,29)} = 9.965$, $p = 0.003$, $\eta^2 = 0.407$; Kruskal–Wallis, $H_{(2)} = 11.366$, $p = 0.017$). The EE group showed significantly greater PSC than the SC group ($p < 0.001$) but not the BC group ($p = 0.069$; but $p = 0.018$ with BC6 excluded). The BC and SC groups did not differ ($p = 0.071$). None of the other ROIs showed a significant group effect (A1, $F_{(2,29)} = 2.337$, $p = 0.573$; Kruskal–Wallis, $H_{(2)} = 5.030$, $p = 0.404$; PHPA, $F_{(2,29)} = 1.224$, $p = 1.000$; Kruskal–Wallis, $H_{(2)} = 3.331$, $p = 0.945$; SPL, $F_{(2,29)} = 0.801$, $p = 1.000$; Kruskal–Wallis, $H_{(2)} = 1.152$, $p = 1.000$).

PSC in A1 was significantly greater than zero for the SC group ($t(13) = 9.313$, $p < 0.001$; Wilcoxon signed rank, $z = 3.296$, $p < 0.001$), BC group ($t_{(11)} = 3.174$, $p = 0.009$; Wilcoxon signed rank, $z = 2.197$, $p = 0.028$), and EE group ($t_{(5)} = 4.626$, $p = 0.006$; Wilcoxon signed rank, $z = 2.201$, $p = 0.028$). PSC in V1 was significantly greater than zero for the EE group ($t_{(5)} = 4.394$, $p = 0.007$; Wilcoxon signed rank, $z = 2.201$, $p = 0.028$). PSC in PHPA was significantly lower than zero for the SC group ($t_{(13)} = 3.631$, $p = 0.003$; Wilcoxon signed rank, $z = 2.794$, $p = 0.005$). PSC in the OPA was significantly greater than zero for the EE group ($t_{(5)} = 3.495$, $p = 0.017$; Wilcoxon signed rank, $z = 2.201$, $p = 0.028$). No other tests showed a significant difference from zero.

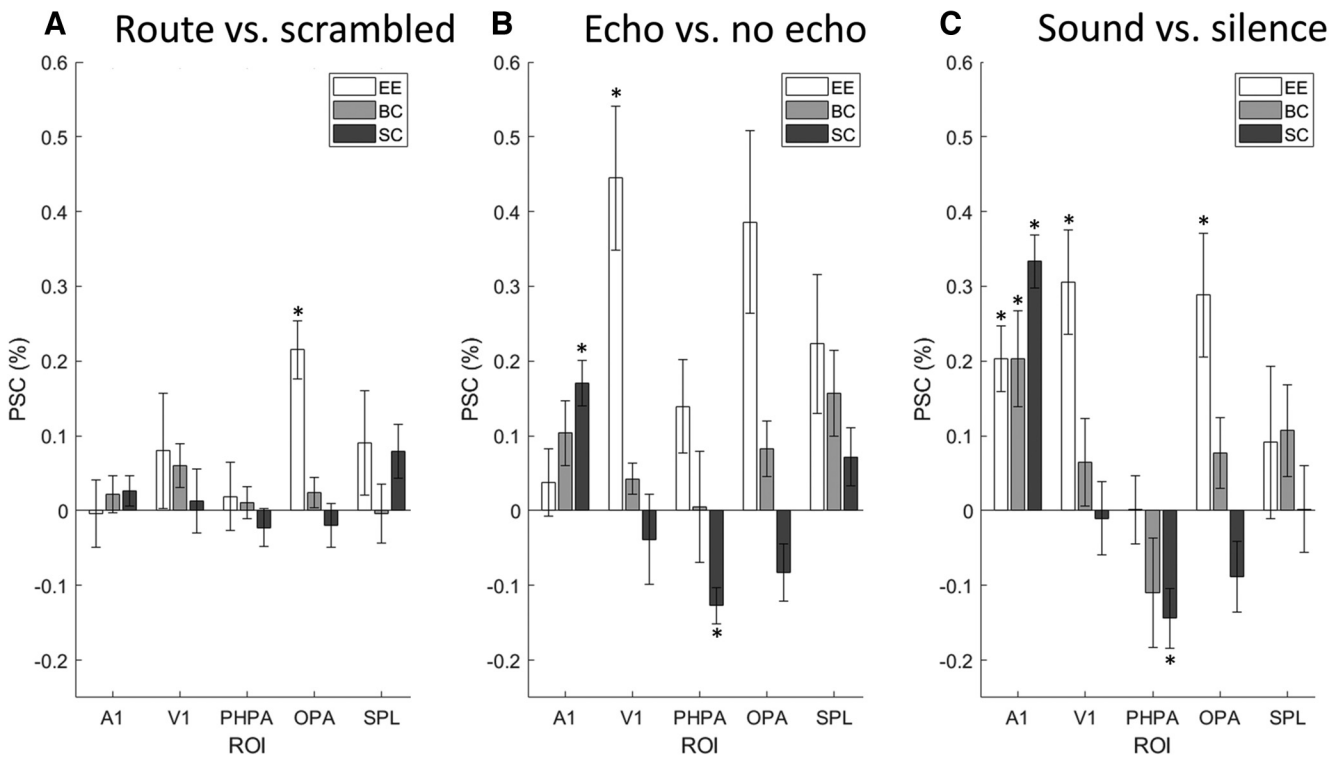

Figure 3. ***A–C***, Results of the ROI analysis for route versus scrambled (***A***), echo versus no echo (***B***), and sound versus silence (***C***) contrasts. PSC is shown for each contrast, ROI, and participant group. Error bars indicate SEM. Asterisks indicate where the PSC for that ROI was significantly different from zero after applying the Benjamini-Hochberg method (FDR set to 0.05). Table 3 contains the individual data for the six EEs.

Additional ROI analyses: OPA activity and echolocation ability

It is possible that the activity observed in the OPA is only driven by high performance on the route versus scrambled identification task, regardless of participants being EEs, BCs, or SCs. In our study, BC and SC groups were, expectedly, less accurate on this task than the EE group. Thus, to address the possibility that OPA activity in EEs is because of their more accurate task performance, we ran two further analyses. First, we reran the route versus scrambled contrast analysis only using trials in which participants had classified correctly. To avoid differences in statistical power between EEs and controls, we subsampled data from EEs to match number of trials across groups. Analyzing PSC in the OPA using only correct trials showed the same pattern of results that we found when using all trials (EEs mean = 0.26, BCs mean = 0.10, SCs mean = −0.02), and there was a significant difference among groups ($F_{(2,29)}$ = 9.562, p = 0.003, η^2 = 0.397; Kruskal–Wallis, $H_{(2)}$ = 12.948, p = 0.008), with EEs showing a significantly greater response compared with SCs ($p < 0.001$) but not BCs (p = 0.067). BCs and SCs were not significantly different from one another (p = 0.090). Applying the Benjamini–Hochberg method, only the EE group showed a response in the OPA significantly greater than zero ($t_{(5)}$ = 5.604, p = 0.003; Wilcoxon signed rank, z = 2.201, p = 0.028). Second, to further investigate possible associations between behavioral performance and OPA response (for the route vs scrambled contrast), we ran a correlation analysis that revealed for EEs a borderline significant correlation between behavioral performance and PSC in the OPA ($r_{(4)}$ = 0.808, p = 0.052), but no correlation for BCs ($r_{(10)}$ = 0.361, p = 0.249) or SCs ($r_{(12)}$ = −0.001, p = 0.998). Figure 4 shows the scatter plot of these data. These results suggest that responses in the OPA are not driven solely by the ability to identify route versus scrambled sounds but is likely the result of both long-term echolocation experience and task-specific echolocation ability.

Table 3. Individual PSC data points for the six EEs, organized by contrast and ROI

	A1	V1	PHPA	OPA	SPL
Route vs scrambled					
EE1	0.14	0.27	−0.01	0.23	0.31
EE2	−0.09	−0.24	−0.18	0.24	−0.12
EE3	−0.02	0.05	0.04	0.05	0.06
EE4	−0.02	0.10	0.03	0.18	0.18
EE5	−0.14	0.27	0.16	0.33	−0.08
EE6	0.11	0.03	0.07	0.26	0.20
Echo vs no echo					
EE1	0.19	0.16	0.27	0.06	0.11
EE2	0.02	0.48	0.14	0.20	−0.09
EE3	0.09	0.27	−0.08	0.14	0.14
EE4	0.10	0.32	0.01	0.54	0.31
EE5	−0.11	0.71	0.17	0.82	0.29
EE6	−0.07	0.73	0.33	0.56	0.58
Sound vs silence					
EE1	0.37	0.27	−0.09	0.24	0.25
EE2	0.30	0.10	0.20	0.10	−0.34
EE3	0.12	0.17	−0.09	0.01	0.01
EE4	0.15	0.27	−0.07	0.49	0.28
EE5	0.16	0.53	0.06	0.47	0.03
EE6	0.11	0.49	0.00	0.41	0.32

Group means of these data are shown in Figure 3.

Additional ROI analyses: functionally localized OPA ROI

In the sighted brain, the location of the OPA is typically defined using a functional localizer comparing static visual scenes to static visual objects (Sun et al., 2021; Kamps et al., 2016; Dilks et

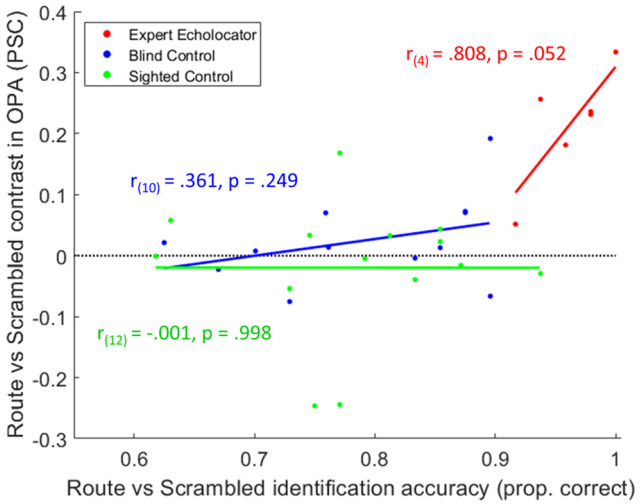

Figure 4. The association between the PSC in OPA for the route versus scrambled contrast (*y*-axis) and perceptual identification accuracy of route versus scrambled sounds (*x*-axis). Each point represents an individual subject, with separate groups denoted by different colors. The solid lines show linear model fits.

al., 2013). In our study, this region was defined as a single sphere centered on the average MNI coordinates from an independent study that used the functional localizer in 17 sighted subjects (Sun et al., 2021). To verify that our observed activation in the OPA in EEs corresponds to the functionally defined OPA, we conducted an additional analysis using localizer data for 14 sighted adults from a second independent study (Meissner et al., 2019). The raw data were obtained through Open Science Framework (https://osf.io/aydqz/) and analyzed using FSL FEAT preprocessing (brain extraction, nonlinear registration at 2 mm resolution, slice-timing correction, motion correction, high-pass temporal filtering at 70 s, and spatial smoothing at 5 mm) and mixed effects statistical model. The group-level statistical map for the contrast scenes versus objects was thresholded using clusters determined by $Z > 4.00$ and a (corrected) cluster significance threshold of $p = 0.05$, and we used this result to identify two clusters in occipital cortex that were centered at approximately spatially mirrored locations across the left and right hemispheres (left, −36, −74, 26; number of voxels = 153; right, 34, −78, 20; number of voxels = 166). The coordinates of those clusters corresponded well to those from Sun et al. (2021; left, −29.4, −83.8, 23.9; right, 35.7, −78.5, 23.7). We then used these cluster masks as ROIs to analyze PSC for the route versus scrambled contrast. Replicating our original finding, EEs showed a significant response for route versus scrambled in left ($t_{(5)} = 3.930$, $p = 0.011$; Wilcoxon signed rank, $z = 2.201$, $p = 0.028$) and right hemisphere ROIs ($t_{(5)} = 5.074$, $p = 0.004$; Wilcoxon signed rank, $z = 2.201$, $p = 0.028$).

Additional ROI analyses: PSC for individual stimulus conditions

Furthermore, to determine the nature of the effect(s) underlying the response in the OPA in EEs, we analyzed the PSC in this area in response to each of the three individual stimulus conditions (i.e., relative to silence baseline) and compared these with the same values in control regions A1 and V1. These values (and those for all ROIs) are shown in Figure 5. In a two-way within-subject ANOVA with the factors ROI (OPA, A1, V1) and stimulus (route, scrambled, no echo), there was a significant interaction ($F_{(4,20)} = 5.446$, $p = 0.004$, $\eta_p^2 = 0.521$). This implies a difference in response profiles across the three ROIs to the different stimuli. This was further explored in separate ANOVAs for each ROI. In the OPA there was a significant difference between stimulus conditions ($F_{(2,10)} = 11.457$, $p = 0.003$, $\eta_p^2 = 0.696$), with route sounds evoking greater PSC compared with no-echo sounds ($t_{(5)} = 3.674$, $p = 0.014$) and scrambled sounds ($t_{(5)} = 5.613$, $p = 0.002$). Scrambled sounds did not evoke significantly stronger PSC compared with no-echo sounds ($t_{(5)} = 2.479$, $p = 0.056$). In contrast, in A1 there was no significant difference between stimulus conditions ($F_{(2,10)} = 0.371$, $p = 0.699$). In V1, there was a significant difference ($F_{(2,10)} = 14.725$, $p = 0.001$, $\eta_p^2 = 0.747$), with route sounds evoking greater PSC compared with no-echo sounds ($t_{(5)} = 4.907$, $p = 0.004$) but not scrambled sounds ($t_{(5)} = 1.054$, $p = 0.340$), although scrambled sounds did evoke greater PSC compared with no-echo sounds ($t_{(5)} = 3.727$, $p = 0.014$). Furthermore, we were able to validate using one-sample *t* tests (applying the Benjamini–Hochberg method, as previously described) that in OPA route sounds evoked activity significantly greater than zero ($t_{(5)} = 3.988$, $p = 0.010$; Wilcoxon signed rank, $z = 2.201$, $p = 0.028$), whereas neither scrambled ($t_{(5)} = 2.889$, $p = 0.034$; note that this is a nonsignificant result when p value is compared against the Benjamini–Hochberg critical value of 0.023; Wilcoxon signed rank, $z = 2.201$, $p = 0.028$) nor no-echo sounds ($t_{(5)} = 0.685$, $p = 0.524$; Wilcoxon signed rank, $z = 0.524$, $p = 0.600$) led to significant activity. All significant one-sample *t* tests are displayed in Figure 5.

For BCs, the same analysis did not reveal a significant interaction between stimulus condition and ROI ($F_{(4,44)} = 0.729$, $p = 0.577$). For SCs, there was a significant interaction ($F_{(4,52)} = 11.003$, $p < 0.001$, $\eta_p^2 = 0.458$). Further ANOVAs revealed that in the OPA there was a significant difference between stimulus conditions ($F_{(2,10)} = 3.468$, $p = 0.046$, $\eta_p^2 = 0.211$), with route sounds evoking less PSC compared with no-echo sounds ($t_{(5)} = 2.194$ $p = 0.047$). There was no difference between scrambled sounds and route sounds ($t_{(5)} = 0.693$, $p = 0.500$) or between scrambled sounds and no-echo sounds ($t_{(5)} = 1.881$, $p = 0.083$). In A1 there was also significant difference between conditions ($F_{(2,26)} = 24.034$, $p < 0.001$, $\eta_p^2 = 0.649$), which was driven by click sounds evoking less PSC compared with both scrambled ($t_{(13)} = 5.109$, $p < 0.001$) and route sounds ($t_{(13)} = 5.572$, $p < 0.001$), but no difference between scrambled and route sounds ($t_{(13)} = 1.273$, $p = 0.225$). There was no significant difference between stimulus conditions in V1 ($F_{(2,26)} = 0.344$, $p = 0.712$). Neither BCs nor SCs showed significant PSC in the OPA in response to any of the stimulus conditions.

Overall, these results show that the OPA in EEs has a unique response profile across the three stimulus conditions compared with the other ROIs and to the other control groups. This response profile is consistent with its role in processing spatially coherent echo-acoustic sounds for navigation.

fMRI: whole-brain analysis

Route versus scrambled

Results for the analysis of a group difference for the route versus scrambled contrast on the whole brain are shown in Figure 6. These results reveal significant clusters in and around the OPA ROI and other occipital and parietal regions. Separate whole-brain activation maps for each subject group are shown in Figure 7. For this contrast, EEs showed two activation clusters. The largest was centered on the superior parietal lobule (subregion 7P) in the left hemisphere, and the other was centred on the inferior parietal lobule (subregion PGp) in the right hemisphere. Both of these clusters extend into the OPA region and are therefore

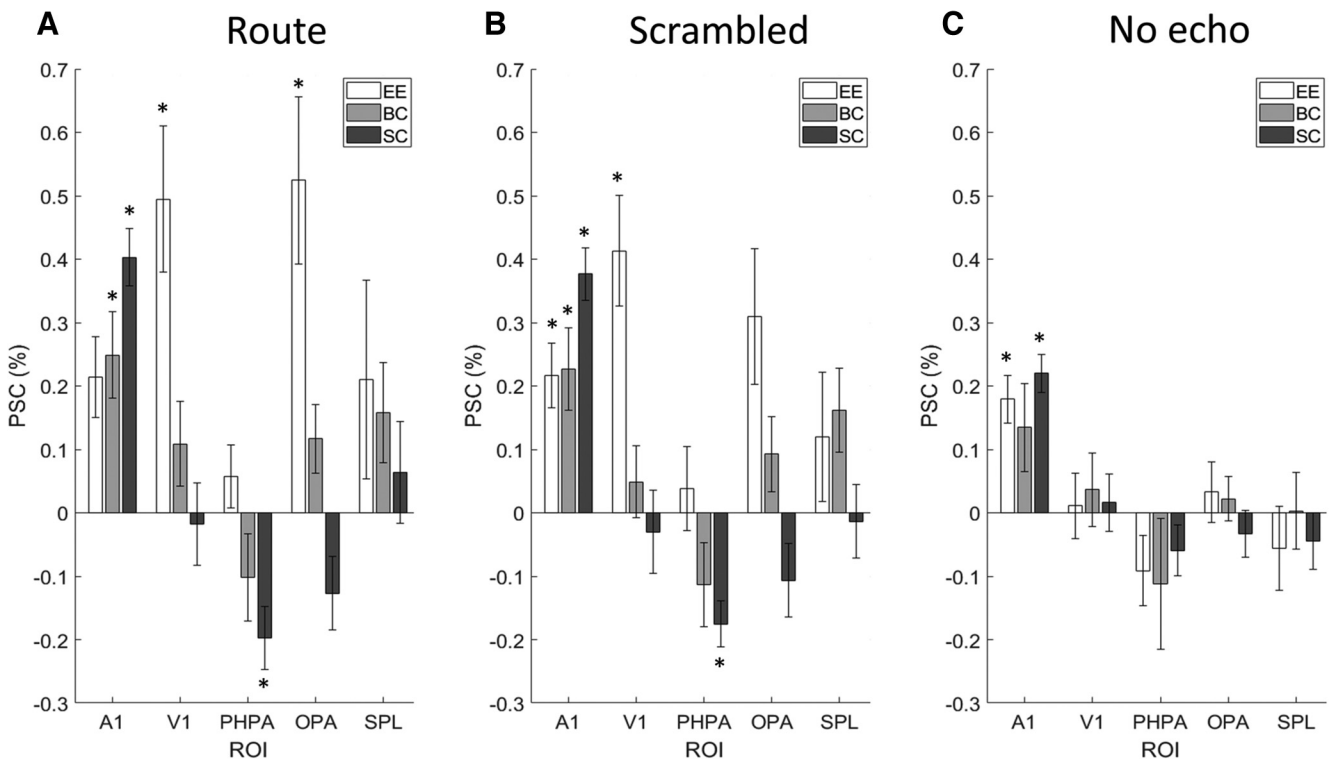

Figure 5. ***A–C***, Results of the ROI analysis for the individual stimulus conditions (i.e., EVs relative to silence baseline), route sound (***A***), scrambled sound (***B***), and no-echo sound (***C***). PSC is shown for each contrast, ROI, and participant group. Asterisks indicate where the PSC for that ROI was significantly different from zero, after applying the Benjamini-Hochberg method (FDR set to 0.05).

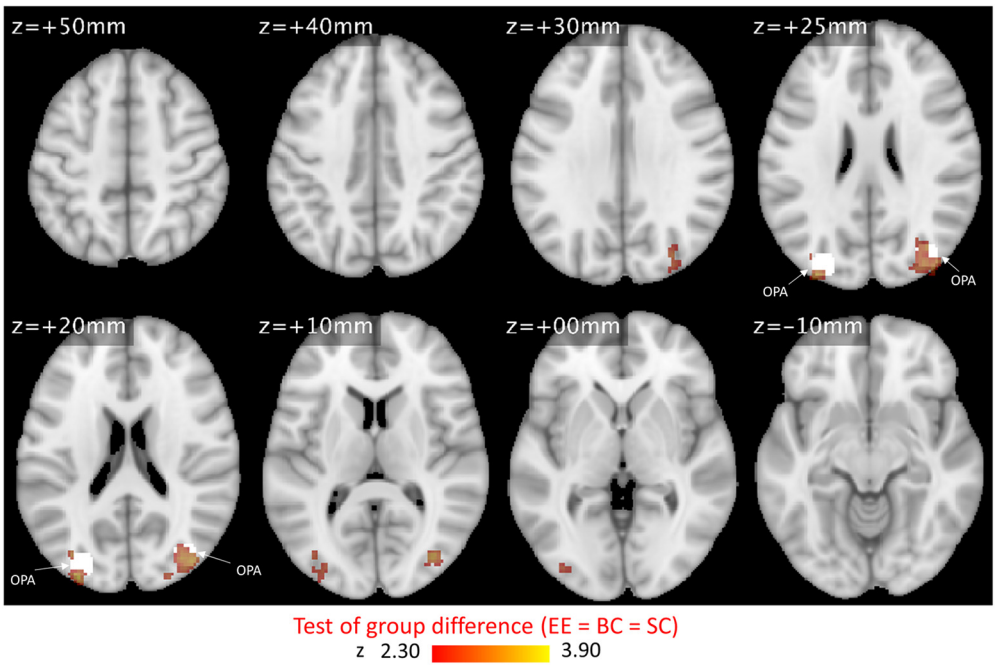

Figure 6. Activation maps showing locations of significant group difference for the contrast route versus scrambled (cluster level threshold of $z > 2.3$ and $p < 0.05$) displayed on the MNI 152 standard-space template. The OPA ROI is visible in white in the cross-sectional slices for $Z = +20$ and $+25$ mm. Orientation of the images is in neurologic convention (i.e., left is left).

consistent with the findings from our ROI analysis. BCs did not show any significant clusters. SCs, however, did show four significant clusters. Three of these covered similar areas identified in EEs (i.e., superior/inferior parietal lobules), in addition to anterior parietal sulcus and some frontal areas (motor cortex and Broca's area). None of the activation clusters for SCs extended into the OPA region. A detailed summary of the activation clusters found for the route versus scrambled contrast is provided in Table 4.

We also quantified the degree of spatial overlap between the cluster maps for the EE route versus scrambled contrast and the functionally defined OPA ROI resulting from the analysis of Meissner et al.'s (2019) sighted localizer data (see above, Additional ROI analyses: functionally localized OPA ROI for

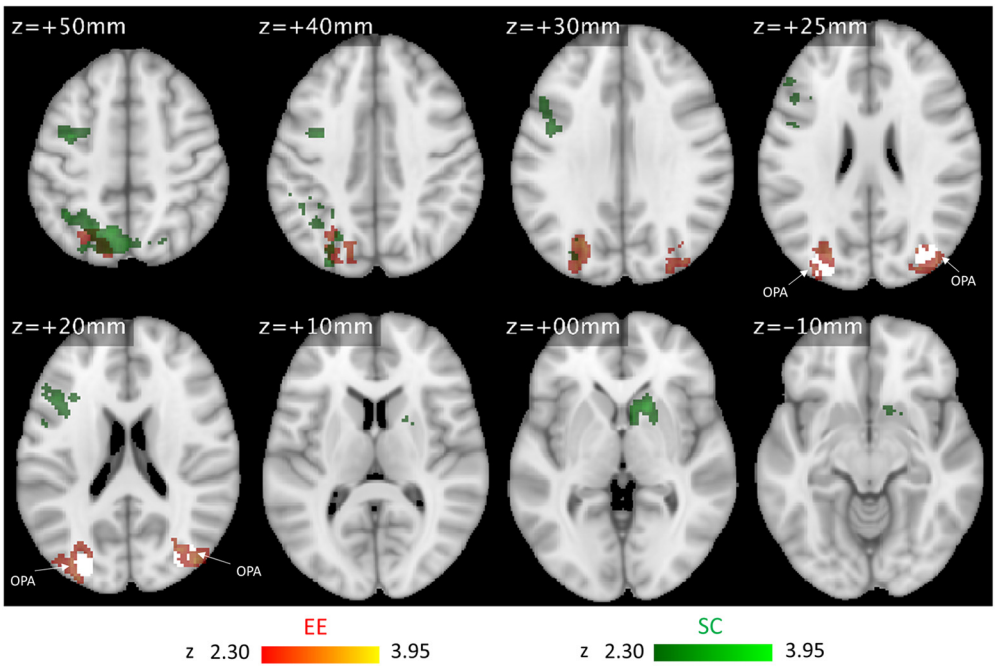

Figure 7. Activation maps for the contrast route versus scrambled (cluster level threshold of $z > 2.3$ and $p < 0.05$) displayed on the MNI 152 standard-space template. Separate color overlays are used to show results from EEs, BCs, and SCs. (Note, there were no significant clusters for BCs.) The color map used to display each overlay is scaled such that they all have the same upper bound (determined by the largest z value in all three overlays). The OPA ROI is visible in white in the cross-sectional slices for $Z = +20$ and $+25$ mm. Orientation of the images is in neurologic convention (i.e., left is left).

Table 4. Route versus scrambled contrast clusters

Subject group	Cluster	Region label	MNI coordinates (mm)			z-Statistic	Number of voxels
			x	y	z		
EEs	1	GM superior parietal lobule 7P L (continuous with OPA)	−24	−72	28	3.14	899
	2	GM inferior parietal lobule PGp R (continuous with OPA)	42	−82	20	3.21	325
BCs	n/a	n/a	n/a	n/a	n/a	n/a	n/a
SCs	1	GM inferior parietal lobule PGp L GM superior parietal lobule 7A L GM Superior parietal lobule 7P L	−18	−66	62	3.95	1370
	2	GM Broca's area BA44 L GM Broca's area BA45 L GM Premotor cortex BA6 L	−46	20	16	3.91	790
	3	Caudate	14	14	−4	3.85	423
	4	GM Anterior intraparietal sulcus hIP3 R GM Superior parietal lobule 7A R GM Superior parietal lobule 7P R	28	−58	58	3.42	320

Summary of peak activations within each cluster for the route versus scrambled contrast. GM, Grey matter; L, Left; R, right; n/a, not applicable.

cluster description). In the right hemisphere, the spatial overlap covered 77 voxels (46% of all voxels in the sighted localizer cluster and 25% of the route versus scrambled cluster in EEs) In the left hemisphere, the spatial overlap covered 32 voxels (21% of voxels in the sighted localizer cluster and 4% of the route versus scrambled cluster in EEs). The low percentage of overlap in EEs in the left hemisphere is attributable to the fact that this cluster in EEs is comparably larger, extending farther into the parietal lobe (compare Table 4 and Fig. 7).

Echo versus no echo

Results for the analysis of a group difference for the echo versus no-echo contrast on the whole brain are shown in Figure 8. These results reveal large areas of activation in occipital and parietal cortex. Separate whole-brain activation maps for each subject group are shown in Figure 9. The pattern of results was similar across BCs and SCs and included primary auditory cortex, premotor cortex, and parietal areas (anterior intraparietal sulcus and superior/inferior parietal lobules). There were also significant activation clusters in Broca's areas in both groups. The pattern of activity observed for the EE group included similar areas that were activated in the BC and SC groups but additionally included a large activation cluster in early visual cortex. Detailed descriptions of these clusters are shown in Table 5.

Sound versus silence

Results for the analysis of a group difference for the sound versus silence contrast on the whole brain are shown in Figure 10. These results reveal similar areas of activation to the echo versus no-echo contrast. Separate whole-brain activation maps for each subject group are shown in Figure 11. All three groups showed significant activation clusters in a number of different brain areas

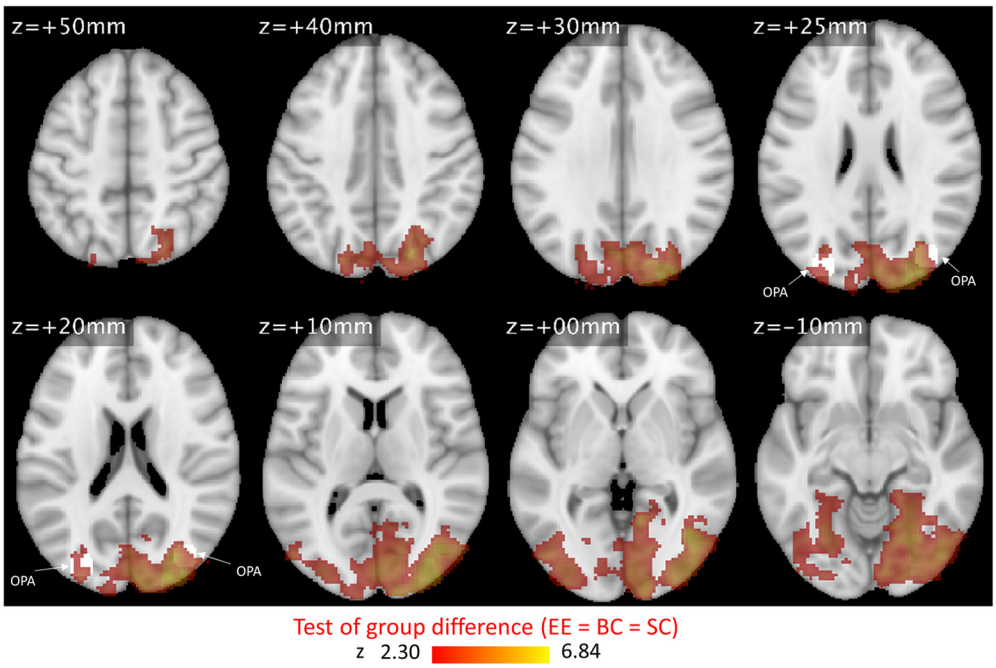

Figure 8. As Figure 6, but for the contrast echo versus no echo.

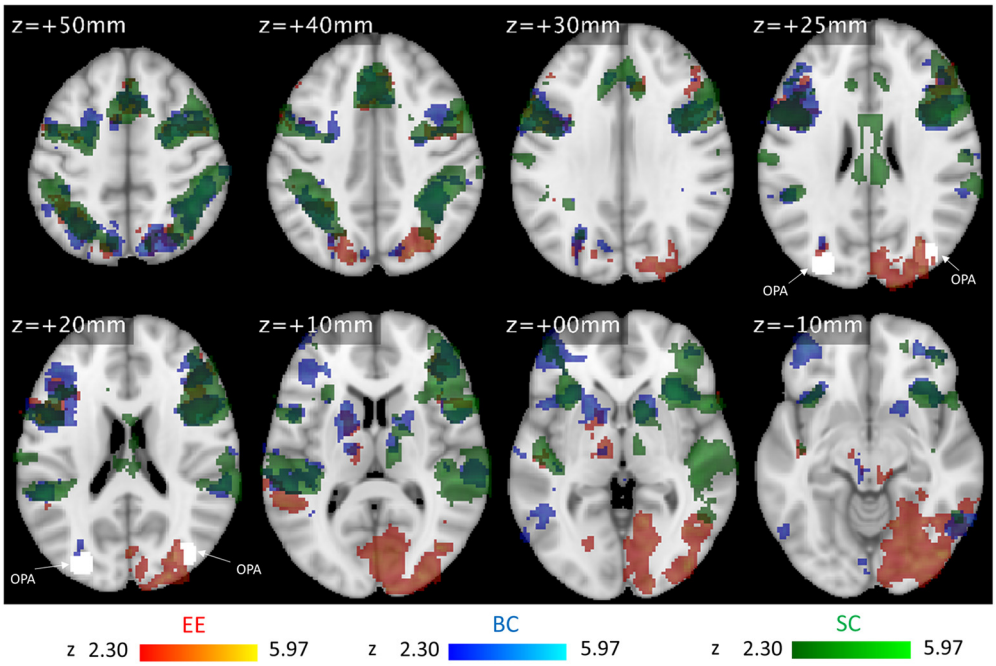

Figure 9. As Figure 7, but for the contrast echo versus no echo.

(This is to be expected, based on the nonspecific nature of the contrast.). Most notably, these activation clusters included primary auditory cortex, motor/premotor cortex, and parietal areas (anterior parietal sulcus and superior/inferior parietal lobules). The EE group was the only group that also showed a significant activation cluster in early visual cortex. Detailed descriptions of these clusters are provided in Table 6.

Discussion

In the present study, we have shown that the OPA is recruited in blind EEs during traversal of a virtual echo-acoustic space in first-person perspective. This was not found in blind or sighted controls (BCs or SCs, respectively). The task we used can be considered an echo-acoustic analog of a vision-based task that has previously been found to evoke activation in the OPA in sighted people (Kamps et al., 2016). Our study, therefore, provides evidence that the OPA is not uniquely associated with visually guided navigation but can also be similarly recruited for echo-acoustic navigation. ROI and whole-brain analyses provided converging evidence for OPA involvement, and our behavioral measures verified that EEs could discriminate coherent route sounds from scrambled sounds. Further, the critical contrast was

Table 5. Echo versus no-echo contrast clusters

Subject group	Cluster	Region label	MNI coordinates (mm)			*z*-Statistic	Number of voxels
			x	*y*	*z*		
EEs	1	GM visual cortex V2 BA18 R GM visual cortex V3V R	34	−88	22	4.51	11224
	2	GM premotor cortex BA6 R	40	−2	46	4.51	2163
	3	GM anterior intraparietal sulcus hIP3 L GM inferior parietal lobule PFm L GM inferior parietal lobule Pga L GM superior parietal lobule 7A L	−30	−58	54	4.09	1504
	4	GM Broca's area BA44 L GM Broca's area BA45 L	−50	8	28	4.07	1307
	5	GM premotor cortex BA6 R	−4	18	44	4.27	794
	6	Thalamus	−12	−14	0	3.36	731
	7	Temporal lobe	−50	−48	12	4.12	622
BCs	1	Cerebellum Temporal lobe	52	−62	−12	4.23	6047
	2	GM Broca's area BA45 L GM Premotor cortex BA6 L	−42	52	−4	4.49	3959
	3	Frontal lobe	30	26	0	4.64	3873
	4	GM Anterior intraparietal sulcus hIP2 R GM anterior intraparietal sulcus hIP3 R GM inferior parietal lobule PF R GM inferior parietal lobule PFm R GM auperior parietal lobule 7P R	50	−40	58	4.59	2031
	5	GM anterior intraparietal sulcus hIP1 L GM anterior intraparietal sulcus hIP3 L GM inferior parietal lobule Pga L GM primary somatosensory cortex BA2 L GM superior parietal lobule 7A L GM superior parietal lobule 7P L	−32	−60	44	4.21	1880
	6	Frontal lobe Insula Putamen	−36	18	−2	4.3	938
	7	GM inferior parietal lobule PFcm L GM primary auditory cortex TE1.1 L	−50	−40	20	4.28	925
	8	GM premotor cortex BA6 R	−4	20	44	5.13	791
	9	GM inferior parietal lobule PF R GM inferior parietal lobule PFcm R	66	−30	8	3.94	533
	10	Putamen Thalamus	20	12	−10	3.42	515
	11	Inferior temporal gyrus, temporooccipital part Lateral occipital cortex, inferior division Middle TEMPORAL Gyrus, temporooccipital part	−52	−54	8	3.75	308
SCs	1	GM Broca's area BA44 R GM Broca's area BA45 R	46	8	24	5.96	10360
	2	GM anterior intraparietal sulcus hIP1 L GM inferior parietal lobule Pga L GM insula Id1 L GM primary somatosensory cortex BA1 L GM primary somatosensory cortex BA2 L	−46	−38	56	5.11	4597
	3	GM anterior intraparietal sulcus hIP1 R GM anterior intraparietal sulcus hIP2 R GM anterior intraparietal sulcus hIP3 R GM inferior parietal lobule PF R GM inferior parietal lobule PFm R GM inferior parietal lobule PFt R GM primary somatosensory cortex BA1 R GM primary somatosensory cortex BA2 R	48	−38	52	5.45	3123
	4	GM inferior parietal lobule PF R GM Primary auditory cortex TE1.1 R	50	−32	8	4.73	2951
	5	GM Broca's area BA44 L GM premotor cortex BA6 L	−58	6	28	5.31	2785
	6	Cerebellum	−10	−82	−30	5.62	1981
	7	Thalamus	12	10	2	4.78	1121
	8	Frontal orbital cortex	−36	28	2	4.77	805

(*Table continues*.)

Table 5 Continued

Subject group	Cluster	Region label	MNI coordinates (mm)			*z*-Statistic	Number of voxels
			x	*y*	*z*		
	9	Frontal pole Insular cortex Cerebellum	14	−78	−46	4.13	440

As Table 4, but for the echo versus no-echo contrast. GM, gray matter; L, Left; R, right.

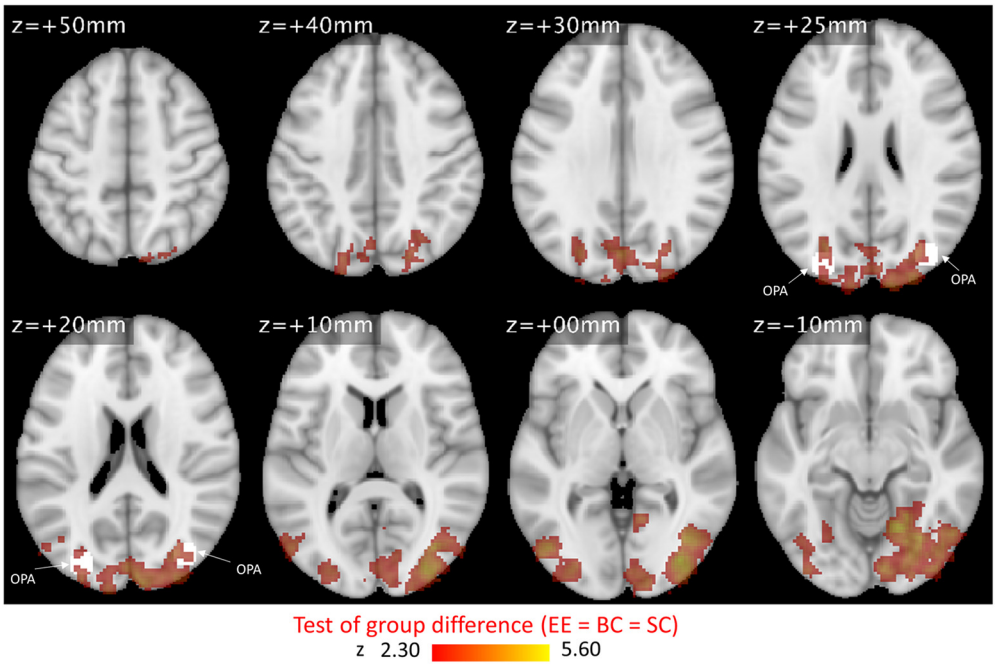

Figure 10. As Figures 6 and 8, but for the contrast sound versus silence.

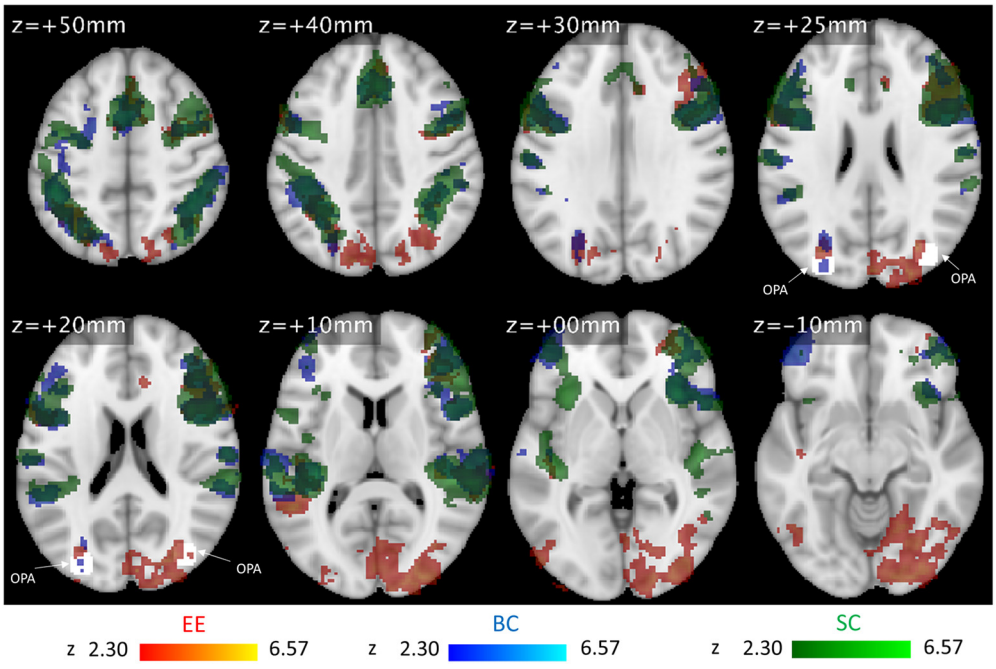

Figure 11. As Figures 7 and 9, but for the contrast sound versus silence.

Table 6. Sound versus silence contrast clusters

Subject group	Cluster	Region label	MNI coordinates (mm)			z-Statistic	Number of voxels
			x	y	z		
EEs	1	GM visual cortex V2 BA18 R	36	−90	6	4.2	7745
	2	GM Broca's area BA44 R	42	12	20	4.25	2636
		GM Broca's area BA45 R					
		GM premotor cortex BA6 R					
	3	GM anterior intraparietal sulcus hIP3 L	−34	−58	54	4.08	1987
		GM superior parietal lobule 7A L					
		GM superior parietal lobule 7P L					
	4	GM premotor cortex BA6 R	6	26	42	4.04	728
		GM inferior parietal lobule PFcm L					
		GM primary auditory cortex TE1.0 L					
		GM primary auditory cortex TE1.1 L					
		WM acoustic radiation L					
	5	GM inferior parietal lobule PFcm L	−50	−48	8	4.32	628
		GM primary auditory cortex TE1.0 L					
		GM primary auditory cortex TE1.1 L					
		WM acoustic radiation L					
	6	GM Broca's area BA44 L	−58	12	22	3.86	539
		GM premotor cortex BA6 L					
	7	GM inferior parietal lobule PF R	62	−36	12	4.19	437
		GM primary auditory cortex TE1.0 R					
		GM primary auditory cortex TE1.1 R					
		WM acoustic radiation R					
BCs	1	GM anterior intraparietal sulcus hIP3 L	−42	−36	46	5.24	6653
		GM primary somatosensory cortex BA1 L					
		GM primary somatosensory cortex BA2 L					
		GM primary somatosensory cortex BA3b L					
	2	Frontal lobe	36	22	0	4.83	4237
		Insula					
	3	GM anterior intraparietal sulcus hIP2 R	42	−42	50	4.34	1370
		GM anterior intraparietal sulcus hIP3 R					
		GM inferior parietal lobule PF R					
		GM inferior parietal lobule PFm R					
		GM superior parietal lobule 7A R					
		GM superior parietal lobule 7P R					
		GM superior parietal lobule 7PC R					
	4	GM inferior parietal lobule PFcm L	−46	−38	18	4.31	1271
		GM Primary auditory cortex TE1.0 L					
		GM primary auditory cortex TE1.1 L					
		GM secondary somatosensory cortex/parietal operculum OP1 L					
		WM acoustic radiation L					
	5	GM inferior parietal lobule PF R	62	−34	12	5.15	1021
		GM primary auditory cortex TE1.1 R					
		GM secondary somatosensory cortex/parietal operculum OP1 R					
		GM secondary somatosensory cortex/parietal operculum OP4 R					
SCs	1	GM anterior intraparietal sulcus hIP1 L	−36	−28	10	6.57	8164
		GM anterior intraparietal sulcus hIP3 L					
		GM inferior parietal lobule PFcm L					
		GM insula Ig1 L					
		GM insula Ig2 L					
		GM primary auditory cortex TE1.1 L					
		GM primary somatosensory cortex BA2 L					
		WM acoustic radiation L					
	2	GM Broca's area BA44 R	38	0	50	5.58	7588
	3	GM primary auditory cortex TE1.0 R	46	−26	8	5.54	2377
		GM primary auditory cortex TE1.1 R					
		WM acoustic radiation R					
	4	GM premotor cortex BA6 R	−2	32	40	5.27	2153
	5	GM anterior intraparietal sulcus hIP1 R	38	−54	42	5.83	2123
		GM anterior intraparietal sulcus hIP2 R					
		GM anterior intraparietal sulcus hIP3 R					
		GM inferior parietal lobule PFm R					
		GM inferior parietal lobule Pga R					
	6	Frontal lobe	−34	18	−2	4.94	1047

(*Table continues*.)

Table 6 Continued

Subject group	Cluster	Region label	MNI coordinates (mm)			z-Statistic	Number of voxels
			x	y	z		
		Insula					
	7	Cerebellum	−12	−78	−22	4.74	806

As in Tables 4 and 5, but for the sound versus silence contrast. GM, gray matter; L, Left; R, right.

based on sounds that controlled for spectrotemporal acoustic properties.

The OPA has been previously identified as an important part of the human navigation brain network, being associated with visual perception of static scenes (Dilks et al., 2013) as well as dynamic boundary-based spatial navigation (Kamps et al., 2016; Julian et al., 2016). Julian et al. (2016), for example, used TMS to show that in sighted people the OPA is causally involved in the encoding of object locations relative to boundaries in the environment. Specifically, they hypothesize that the OPA serves as the source of the perceptual representation of environmental boundary information, which is then used in the spatial coding of the environment in the larger network of navigation-related brain regions. It is also known that the OPA and PHPA are functionally connected (Baldassano et al., 2013), which might mediate input form the OPA to the hippocampal formation (Naber et al., 1997). What the present study demonstrates, however, is that the perceptual representation formed in the OPA is not necessarily formed through visual input and can also be formed in the absence of vision.

Participants in the BC but not EE group tended to have some residual visual sensitivity. It is thus possible that complete blindness itself, rather than echolocation experience, is sufficient to elicit OPA responses to echo-acoustic sounds. In this context it is important to note that our BCs and SCs were very similar in their brain activations, whereas both groups differed greatly from EEs. This suggests that long-term experience in echolocation rather than blindness per se underlies the response in the OPA. Furthermore, our additional analyses also suggested that the activity in the OPA was unique to EEs and not simply driven by participants' accuracy at identifying route versus scrambled sounds, regardless of them being EEs, BCs, or SCs. Specifically, our data suggested that although OPA activity was significantly higher for EEs compared with the control groups there was no evidence in the control groups that this activity was predicted by their task performance. In contrast, the pattern of results within the six EEs indicated a positive association (although only borderline statistically significant) between task performance and OPA activity. This dual influence of long-term echolocation experience and task-specific ability is strikingly similar to our previous finding that both long-term echolocation experience and echo-localization acuity predict the degree of retinotopic-like mapping of sounds in V1 (Norman and Thaler, 2019).

With respect to activations in parietal cortices (in particular SPL), our ROI analysis, which considered SPL as combination of subareas 5 Ci, 5L, 5 M, 7A, 7 M, and 7P did not show any significant involvement for any contrast or participant group. Yet, the whole-brain analysis revealed significant clusters of activation for subareas of SPL for different participant groups and contrasts. These activations are generally consistent with those reported in a previous study examining echolocation-based route following Fiehler et al. (2015). The result by Fiehler et al. (2015), however, was based on the contrast echo versus no-echo sounds, but the present results from our route versus scrambled contrast do suggest that the activation in SPL reflects the processing of the coherent spatiotemporal structure of echolocation navigation sounds. The SPL has also been shown to be active in sighted people while solving a vision-based route recognition task and in blind people solving the same task using a sensory substitution device (SSD) (Kupers et al., 2010). The specific functional role that the SPL might play in navigation remains unclear, but it has previously been associated with the egocentric coding of visual space (Galati et al., 2000).

In addition to SPL, both EEs and SCs showed activation in the inferior parietal lobule (area PGp), with SCs showing additional activation in the anterior intraparietal sulcus (aIPS). Fiehler et al. (2015) also found some activation in these areas in SCs, and the aIPS have also previously been associated with egocentric spatial coding (Galati et al., 2000). An earlier study found activation within the visual dorsal stream (i.e., parietal cortex), including a posterior area close to the occipitoparietal sulcus (V6/V6a complex), in both blind and sighted blindfolded participants when using a visual-to-auditory SSD to navigate a virtual environment (after training; Maidenbaum et al., 2018). Together with our results, these findings suggest that there are several areas within parietal cortex that might play a role in navigation (with or without vision). It is important to note, however, that areas of posterior parietal cortex such as aIPS and SPL are more generally also considered to be part of the dorsal frontoparietal attention network (Szczepanski et al., 2013), a network that is thought to control top-down attention to environmental objects and tasks (Corbetta et al., 2008; Corbetta and Shulman, 2002). Although this network is typically described with respect to visual processing, effects of spatial attention within the auditory modality have also been observed in posterior parietal cortex (Shomstein and Yantis, 2006). Thus, it remains unclear whether the activity in these posterior parietal areas reflects processes specific to navigation, the multimodal perception of space, or the effects of spatial attention. It is, of course, possible that these areas contribute to complex tasks such as the one used here in a number of ways.

We found no evidence of positive activity in the parahippocampal place area (PHPA) for the contrast route versus scrambled. The PHPA is considered to be central to the spatial navigation network in humans (i.e., parahippocampal cortex; Hartley et al., 2003, 2014). The absence of activity in our paradigm is consistent with studies using a paradigm similar to ours (Fiehler et al., 2015; Kamps et al., 2016) and is likely the result of the nature of the task requirements. Specifically, participants were not required to navigate previously learned environments or to match routes to those held in memory but were instead required to identify the directions of the turns taken along each route. This task design was chosen so we could include a suitable control condition (scrambled sounds) to rule out activity driven by spectrotemporal properties of the stimuli. Kupers et al. (2010), in contrast, required participants using a visual-to-tactile SSD to explicitly match one of two sample routes to a previous one and found parahippocampal activity in blind participants. Interestingly,

for our echo versus no-echo and sound versus silence contrasts we found evidence of negative activity in the parahippocampal place area in SCs. This is similar to the findings of Maidenbaum et al. (2018) in which negative activity in the medial temporal lobe was found in blind and sighted participants when navigating using a visual-to-auditory SSD. The implication of this negative activity remains unclear.

Both ROI and whole-brain analysis showed activation in occipital cortex, including early visual cortex, in the EE group for the contrast echo versus no-echo. This activation was in addition to activity in other areas, including parietal areas, and Broca's areas, which was present in all three groups. The same pattern of results was also observed for the sound versus silence contrast, for which additional activity was also observed in primary auditory areas of all three groups. This pattern of results strongly suggests that recruitment of V1 for processing of echo-acoustic information is tied to experience with echolocation rather than blindness per se. It is by now well established that the neural correlates of echolocation in EEs include several areas of occipital cortex typically associated with inherently visual functions, including V1 (Arnott et al., 2013; Fiehler et al., 2015; Flanagin et al., 2017; Norman and Thaler, 2019; Milne et al., 2015; Thaler et al., 2011; Thaler et al., 2014; Wallmeier et al., 2015). The results of the present study therefore lend further support to the notion that the organization of the human brain is not strictly tied to specific modalities but organized flexibly according to task demands and shaped by experience with a specific task or computation (e.g., echolocation), rather than sensory experience per se (e.g., blindness; Amedi et al., 2017).

In conclusion, the present study found that the OPA, an area previously assumed to be strongly associated with boundary-based visually guided navigation, is driven in EEs during echo-acoustically guided navigation. This opens up novel ways of understanding the brain areas and networks typically involved in visual spatial navigation.

References

Amedi A, Hofstetter S, Maidenbaum S, Heimler B (2017) Task selectivity as a comprehensive principle for brain organization. Trends Cogn Sci 21:307–310.

Andersson JLR, Jenkinson M., Smith S (2010) Non-linear registration, aka spatial normalisation. Oxford, UK: FMRIB technical report TR07JA2.

Arnott SR, Thaler L, Milne JL, Kish D, Goodale MA (2013) Shape-specific activation of occipital cortex in an early blind echolocation expert. Neuropsychologia 51:938–949.

Baldassano C, Beck DM, Fei-Fei L (2013) Differential connectivity within the parahippocampal place area. Neuroimage 75:228–237.

Beckmann CF, Jenkinson M, Smith SM (2003) General multilevel linear modeling for group analysis in FMRI. Neuroimage 20:1052–1063.

Benjamini Y, Hochberg Y (1995) Controlling the false discovery rate: a practical and powerful approach to multiple testing. J R Stat Soc Series B Stat Methodol 57:289–300.

Boccia M, Nemmi F, Guariglia C (2014) Neuropsychology of environmental navigation in humans: review and meta-analysis of FMRI studies in healthy participants. Neuropsychol Rev 24:236–251.

Brainard DH (1997) The Psychophysics Toolbox. Spatial Vis 10:433–436.

Chan E, Baumann O, Bellgrove MA, Mattingley JB (2012) From objects to landmarks: the function of visual location information in spatial navigation. Front Psychol 3:304.

Collins DL, Holmes CJ, Peters TM, Evans AC (1995) Automatic 3-D model-based neuroanatomical segmentation. Hum Brain Mapp 3:190–208.

Corbetta M, Shulman GL (2002) Control of goal-directed and stimulus-driven attention in the brain. Nat Rev Neurosci 3:201–215.

Corbetta M, Patel G, Shulman GL (2008) The reorienting system of the human brain: from environment to theory of mind. Neuron 58:306–324.

Dilks DD, Julian JB, Paunov AM, Kanwisher N (2013) The occipital place area is causally and selectively involved in scene perception. J Neurosci 33:1331–1336a.

Dodsworth C, Norman LJ, Thaler L (2020) Navigation and perception of spatial layout in virtual echo-acoustic space. Cognition 197:104185.

Eickhoff SB, Paus T, Caspers S, Grosbras MH, Evans AC, Zilles K, Amunts K (2007) Assignment of functional activations to probabilistic cytoarchitectonic areas revisited. Neuroimage 36:511–521.

Ekstrom AD (2015) Why vision is important to how we navigate. Hippocampus 25:731–735.

Ekstrom AD, Huffman DJ, Starrett M (2017) Interacting networks of brain regions underlie human spatial navigation: a review and novel synthesis of the literature. J Neurophysiol 118: 3328–3344.

Epstein R, Harris A, Stanley D, Kanwisher N (1999) The parahippocampal place area: recognition, navigation, or encoding? Neuron 23:115–125.

Fiehler K, Schütz I, Meller T, Thaler L (2015) Neural correlates of human echolocation of path direction during walking. Multisens Res 28:195–226.

Flanagin VL, Schörnich S, Schranner M, Hummel N, Wallmeier L, Wahlberg M, Stephan T, Wiegrebe L (2017) Human exploration of enclosed spaces through echolocation. J Neurosci 37:1614–1627.

Galati G, Lobel E, Vallar G, Berthoz A, Pizzamiglio L, Le Bihan D (2000) The neural basis of egocentric and allocentric coding of space in humans: a functional magnetic resonance study. Exp Brain Res 133:156–164.

Griffin DR (1944) Echolocation by blind men, bats and radar. Science 100:589–590.

Hall DA, Haggard MP, Akeroyd MA, Palmer AR, Summerfield AQ, Elliott MR, Gurney EM, Bowtell RW (1999) "Sparse" temporal sampling in auditory fMRI. Hum Brain Mapp 7:213–223.

Hartley T, Maguire EA, Spiers HJ, Burgess N (2003) The well-worn route and the path less traveled: distinct neural bases of route following and wayfinding in humans. Neuron 37: 877–888.

Hartley T, Lever C, Burgess N, O'Keefe J (2014) Space in the brain: how the hippocampal formation supports spatial cognition. Philos Trans R Soc Lond B Biol Sci 369:20120510.

Jenkinson M, Smith S (2001) A global optimisation method for robust affine registration of brain images. Med Image Anal 5:143–156.

Jenkinson M, Bannister P, Brady M, Smith S (2002) Improved optimization for the robust and accurate linear registration and motion correction of brain images. Neuroimage 17:825–841.

Julian JB, Ryan J, Hamilton RH, Epstein RA (2016) The occipital place area is causally involved in representing environmental boundaries during navigation. Curr Biol 26:1104–1109.

Kamps FS, Lall V, Dilks DD (2016) The occipital place area represents first-person perspective motion information through scenes. Cortex 83:17–26.

Kolarik AJ, Cirstea S, Pardhan S, Moore BC (2014) A summary of research investigating echolocation abilities of blind and sighted humans. Hear Res 310:60–68.

Kong XZ, Wang X, Pu Y, Huang L, Hao X, Zhen Z, Liu J (2017) Human navigation network: the intrinsic functional organization and behavioral relevance. Brain Struct Funct 222: 749–764.

Kupers R, Chebat DR, Madsen KH, Paulson OB, Ptito M (2010) Neural correlates of virtual route recognition in congenital blindness. Proc Natl Acad Sci U S A 107:12716–12721.

Loomis JM, Klatzky RL, Golledge RG (2001) Navigating without vision: basic and applied research. Optom Vis Sci 78:282–289.

Maidenbaum S, Chebat DR, Amedi A (2018) Human navigation without and with vision-the role of visual experience and visual regions. BioRxiv. Online advance publication. Retrieved April 24, 2023.

Mazziotta J, et al. (2001) A probabilistic atlas and reference system for the human brain: International Consortium for Brain Mapping (ICBM). Philos Trans R Soc Lond B Biol Sci 356:1293–1322.

Meissner TW, Nordt M, Weigelt S (2019) Prolonged functional development of the parahippocampal place area and occipital place area. Neuroimage 191:104–115.

Milne JL, Arnott SR, Kish D, Goodale MA, Thaler L (2015) Parahippocampal cortex is involved in material processing via echoes in blind echolocation experts. Vision Res 109:139–148.

Naber PA, Caballero-Bleda M, Jorritsma-Byham B, Witter MP (1997) Parallel input to the hippocampal memory system through peri-and post-rhinal cortices. Neuroreport 8:2617–2621.

Norman LJ, Thaler L (2018) Human echolocation for target detection is more accurate with emissions containing higher spectral frequencies, and this is explained by echo intensity. Iperception 9:2041669518776984.

Norman LJ, Thaler L (2019) Retinotopic-like maps of spatial sound in primary 'visual' cortex of blind human echolocators. Proc Biol Sci 286:20191910.

Norman LJ, Thaler L (2020) Stimulus uncertainty affects perception in human echolocation: timing, level, and spectrum. J Exp Psychol Gen 149:2314–2331.

Norman LJ, Thaler L (2021) Perceptual constancy with a novel sensory skill. J Exp Psychol Hum Percept Perform 47:269–281.

Shomstein S, Yantis S (2006) Parietal cortex mediates voluntary control of spatial and nonspatial auditory attention. J Neurosci 26:435–439.

Smith SM (2002) Fast robust automated brain extraction. Hum Brain Mapp 17:143–155.

Sun L, Frank SM, Epstein RA, Peter UT (2021) The parahippocampal place area and hippocampus encode the spatial significance of landmark objects. Neuroimage 236:118081.

Szczepanski SM, Pinsk MA, Douglas MM, Kastner S, Saalmann YB (2013) Functional and structural architecture of the human dorsal frontoparietal attention network. Proc Natl Acad Sci U S A 110:15806–15811.

Thaler L, Goodale MA (2016) Echolocation in humans: an overview. Wiley Interdiscip Rev Cogn Sci 7:382–393.

Thaler L, Arnott SR, Goodale MA (2011) Neural correlates of natural human echolocation in early and late blind echolocation experts. PLoS One 6: e20162.

Thaler L, Milne JL, Arnott SR, Kish D, Goodale MA (2014) Neural correlates of motion processing through echolocation, source hearing, and vision in blind echolocation experts and sighted echolocation novices. J Neurophysiol 111: 112–127.

Thinus-Blanc C, Gaunet F (1997) Representation of space in blind persons: vision as a spatial sense? Psychol Bull 121:20–42.

Wallmeier L, Kish D, Wiegrebe L, Flanagin VL (2015) Aural localization of silent objects by active human biosonar: neural representations of virtual echo-acoustic space. Eur J Neurosci 41:533–545.

Weiner KS, Barnett MA, Witthoft N, Golarai G, Stigliani A, Kay KN, Gomez J, Natu VS, Amunts K, Zilles K, Grill-Spector K (2018) Defining the most probable location of the parahippocampal place area using cortex-based alignment and cross-validation. Neuroimage 170:373–384.

Woolrich M (2008) Robust group analysis using outlier inference. Neuroimage 41:286–301.

Woolrich MW, Ripley BD, Brady M, Smith SM (2001) Temporal autocorrelation in univariate linear modeling of FMRI data. Neuroimage 14:1370–1386.

Woolrich MW, Behrens TE, Beckmann CF, Jenkinson M, Smith SM (2004) Multilevel linear modelling for FMRI group analysis using Bayesian inference. Neuroimage 21:1732–1747.

Worsley KJ (2001) Statistical analysis of activation images. In: Functional MRI: an introduction to methods (Jezzard P, Matthews PM, Smith SM, eds), pp 251–270. Oxford, UK: Oxford UP.